Competing effects of surface albedo and orographic elevated heating on regional climate

Shineng Hu and William R. Boos

Department of Geology and Geophysics, Yale University, New Haven, CT 06511, USA

Corresponding author: Shineng Hu (shineng.hu@yale.edu)

Key points:

- Land surface albedo in non-polar regions generally increases with surface height.
- The brighter albedo of high surfaces induces cooling that compensates for orographic elevated heating.
- Surfaces with the albedo and elevation of modern peninsular India would enter a local runaway greenhouse regime without ventilation by large-scale winds.

Abstract

All else being equal, a given atmospheric pressure-level is thought to be warmer over a plateau than over surrounding non-elevated terrain because of orographic "elevated heating". However, elevated surfaces are also typically brighter due to reduced vegetation and increased ice cover. Here we assess the degree to which surface albedo compensates for orographic elevated heating. We confirm that land surface albedo generally increases with surface elevation in observations. Using a cloud system-resolving model, we show that increased surface albedo strongly compensates for orographic elevated heating in radiative-convective equilibrium. A non-elevated surface with the albedo of modern India would enter a runaway greenhouse regime without ventilation by monsoonal winds, while a surface with the albedo and elevation of Tibet would achieve a cooler radiative-convective equilibrium. Surface albedo changes may thus be just as important as surface elevation changes for the evolution of low-latitude regional climate throughout Earth's history.

Keywords: Elevated heating, albedo, radiative-convective equilibrium, monsoons, Tibet

1. Introduction

Land surfaces emit sensible and latent heat into the overlying atmospheric column while radiative fluxes typically extract energy, producing a time-mean state in which the specific energy content of the column tends to increase with the elevation of the underlying land surface. This relationship between atmospheric temperature and surface elevation, which is sometimes loosely termed "elevated heating", has been argued to have a profound influence on regional climate [see review by *Yanai and Wu*, 2006]. In particular, continental-scale circulations have been argued to be driven by elevated heating from numerous plateaus, including the Bolivian Plateau [*Rao and Erdogan*, 1989], the Colorado Plateau [*Tang and Reiter*, 1984], the Zagros Plateau in Iran [*Zaitchik et al.*, 2007], and the Tibetan Plateau [*Staff Members of Academia Sinica*, 1958; *Wu et al.*, 2007]. In an extension of earlier pioneering work on the mechanism of elevated heating [*Flohn*, 1953; *Molnar and Emanuel*, 1999], a recent study showed that the magnitude of the elevated heating effect is set by top-of-atmosphere radiative changes dominated by the sensitivity of the moist adiabatic lapse rate to surface height [*Hu and Boos*, 2017].

Elevated heating by the Tibetan Plateau has received much attention because of the great height (4 km) and horizontal extent (2.5 million km^2) of that plateau and because this elevated heating was long held to drive the large-scale South Asian summer monsoon [*Flohn*, 1968; *Hahn and Manabe*, 1975; *Molnar et al.*, 1993]. However, recent studies showed that this plateau is not the dominant heat source in Asia: maximum upper-tropospheric temperatures and low-level moist static energies lie south of the plateau over the non-elevated Indo-Gangetic plain [*Boos and Kuang*, 2010; *Nie et al.*, 2010]. Furthermore, the simulated South Asian summer monsoon changes little when the plateau is removed in climate models, provided the comparatively narrow mountain chains along its southern and western boundaries are preserved to block intrusions of dry air into the region [*Chakraborty et al.*, 2002; 2006; *Boos and Kuang*, 2010; *Ma et al.*, 2014]. Although some studies show that surface heat fluxes from these narrow mountain ranges are important for producing precipitation in northern India [*Wu et al.*, 2012], no recent work has

argued that the broad Tibetan Plateau is the dominant heat source in South Asia. Nevertheless, the question remains: why doesn't Tibet's elevation allow it to act as the region's dominant thermal forcing?

Land surface albedo – the fraction of incident radiation reflected by the surface – is also known to exert a powerful control on regional climate [*Charney*, 1975], but the combined effects of surface albedo and surface elevation on topographic thermal forcings are seldom discussed. As surface elevation increases, land cover in low latitudes typically shifts from evergreen and deciduous forests to grasslands and shrublands, and eventually to bare rock and snow pack [*Friedl et al.*, 2002]. This transition presumably leads to an increase in surface albedo, but the relationship between surface albedo and elevation and its consequence for regional climate has not been systematically investigated.

If there indeed exists a robust albedo-elevation correlation, increased reflection of shortwave radiation by elevated land surfaces might compensate for some or all of the effects of orographic elevated heating. This possibility, however, has not been quantitatively explored. One previous study of the elevated heating effect did conduct a series of simulations with various surface albedos and elevations, but it did not explore the possible compensation between albedo and elevation or assess where observed climates lie in this albedo-elevation parameter space [*Molnar and Emanuel*, 1999]. We address these questions here, using observations of surface albedo and elevation together with cloud system-resolving simulations of radiative-convective equilibrium states.

2. Albedo-Elevation Relationship: Satellite Observations

We use topography from the ETOPO1 one arc-minute global relief dataset [*Amante and Eakins*, 2009], obtained from NOAA NGDC (http://www.ngdc.noaa.gov/mgg/global/). We use the Filled Land Surface Albedo Product generated from MOD43B3 (the official Terra/MODIS-derived Land Surface Albedo Product) [*Moody et al.*, 2005], obtained from NASA MODIS (http://modis-atmos.gsfc.nasa.gov/ALBEDO/). This albedo dataset aggregates satellite observations in a five-year period (2000-2004) and provides albedo for both isotropic ('white-sky') and direct local noon ('black-sky') conditions in a broad band of wavelengths (0.3-5.0μm) for 23 sixteen-day periods per year. Comparison of MODIS albedo with in-situ observations in various regions suggests that this product has mean bias smaller than 0.02 [*Jin et al.*, 2003; *Wang et al.*, 2004].

We first focus on South Asia, where there are large spatial contrasts in orography, vegetation, and surface type (Figure 1a). Indeed, the surface albedo of the Tibetan Plateau is substantially larger than that of the Indian subcontinent, by about 0.07 (about 0.24 versus 0.17, respectively) in May-Aug. This albedo contrast exists throughout the year, reaching a minimum of 0.06 in early September, and is relatively insensitive to whether white-sky or black-sky albedo is used (supporting information Figure S1).

Extending the analysis to all regions within 60°S-60°N, we further find that annual mean land surface albedo generally increases with surface elevation, especially for surfaces higher than 3-4 km (Figure 1b). For surfaces below 1 km, the albedo is positively skewed due to the existence of

large reflective surfaces like the Sahara desert. Still, the median albedo of these low surfaces is smaller than that of higher elevation bins. The Tibetan Plateau and peninsular India have typical combinations of surface albedo and elevation, and they lie near the median line in this albedo-elevation diagram (Figure 1b); this is true even if we exclude data in the red and blue boxes in Figure 1a. Consistent with the aforementioned idea of albedo-elevation compensation, surface albedo does increase with elevation, and investigations of the Tibet-India system may be generalizable to other tropical-subtropical regions with similar topographic contrasts.

3. Albedo-Elevation Compensation: Cloud System-Resolving Simulations

We now use a cloud system-resolving model (CSRM), the System for Atmospheric Modeling (SAM) version 6.3 [*Khairoutdinov and Randall,* 2003], to study albedo-elevation compensation. The model solves the anelastic equations of motion with prognostic total non-precipitating water and total precipitating water. Surface temperature is interactively computed based on a surface energy balance, and surface fluxes are based on bulk aerodynamic formulae with constant surface exchange coefficients and a constant surface wind speed of 7 m/s. As an idealization of a land surface, we use a one meter-deep ocean layer and multiply the latent heat flux by a fraction $\beta = 0.5$ to represent the reduced evaporative efficiency of land compared to ocean. We tested the model sensitivity to β: substantial free-tropospheric cooling occurs when β is reduced below 0.25, as expected for a very dry climate, but there is little sensitivity to β for $\beta \gtrsim 0.25$ (supporting information Figure S2e,f). We use a horizontal domain size of 96 km × 96 km with 3 km horizontal resolution and 64 vertical levels. This domain has roughly the same horizontal area as one grid cell of a typical global climate model and is intended to represent one vertical column of the atmosphere. We impose a flat lower boundary with no horizontal height variance within the domain, and we prescribe no mean circulation.

We use the radiative transfer scheme from the NCAR Community Climate Model [*Kiehl et al.*, 1998], with radiatively active clouds and water vapor. Insolation is set to Earth's annual- and diurnal-mean value at 30°N (~364 W m^{-2}); the model sensitivity to insolation changes can be crudely estimated by the imposed variations in surface albedo described below. Calculations with a separate radiative-convective single-column model [*Caballero*, 2012] show that a reduction in surface albedo of 0.04 produces the same change in net top-of-atmosphere radiative flux as an insolation increase of 11 W m^{-2}, using a basic state with surface pressure of 500 hPa and surface albedo of 0.24. Furthermore, the insolation received by India and the Tibetan Plateau differs by only about 10 W m^{-2} in the May-August mean (supporting information Figure S3).

We use this CSRM to simulate non-rotating radiative-convective equilibrium (RCE) [e.g. *Emanuel*, 1994], a theoretical state that would exist in the absence of large-scale circulations such as monsoons. Although RCE is never achieved in reality, it is a conceptually useful state for the study of climate problems across a range of timescales. For instance, the RCE temperature of a particular column of the atmosphere is sometimes thought of as a forcing for planetary-scale circulations such as monsoons, with the large-scale circulation moving temperatures away from those of the RCE state through adiabatic advection, and radiative-convective processes relaxing each column back toward RCE [*Lindzen and Hou*, 1988; *Schneider*, 2006]. Here RCE was taken to exist when the drift of surface temperature was less than 0.001°C/day, which typically required about 200 days of model time. We simulated a range of RCE states by prescribing

different combinations of surface albedos and surface pressures or, equivalently, surface elevations, to investigate possible compensation between elevated heating and albedo-induced cooling.

We conducted two main sets of experiments centered on the present-day albedo and elevation of the Tibetan Plateau. In the first set, surface albedo is set to 0.24 (near the observed mean for the plateau; Figure 1a), while surface elevation ranges from 0 km to about 6 km (Figure 2a; supporting information Figure S2a,b). We refer to integrations both by surface height and surface pressure, with heights of 0, 1, 2, 3, 4, and 6 km having surface pressures of, respectively, 1008, 890, 790, 710, 600, and 500 hPa. In the second set of experiments, a surface pressure of 600 hPa is prescribed (roughly 4 km in surface elevation; a typical value for Tibet), while surface albedo is varied from 0.16 to 0.40 (Figure 2b; supporting information Figure S2c,d).

When surface elevation is varied, we find that elevated heating exists as expected (Figure 2a). Surface temperature decreases with surface height at a rate of 2.4°C/km, consistent with a previous estimate that used a single-column model with parameterized convection [*Molnar and Emanuel*, 1999]. The fact that surface temperature decreases with surface height is mainly due to the lapse rate effect described in *Hu and Boos* [2017] (i.e. as surface height increases, background pressure decreases, the moist adiabatic lapse rate decreases, the upper troposphere warms, outgoing longwave radiation increases, and thus surface temperature decreases). This lapse rate effect was shown to be stronger than the effects of changes in shortwave scattering by dry air or in the longwave optical depths of CO_2 and H_2O. Since this rate of surface temperature decrease (2.4°C/km) is much smaller than typical moist adiabatic lapse rates (6-10°C/km), the troposphere is warmer over an elevated surface than over a non-elevated surface in RCE, by as much as 20°C for a 5 km change in surface height.

When we increase surface albedo at fixed surface elevation, more shortwave radiation is reflected back to space and air temperature decreases at all levels of the troposphere (Figure 2b). Moisture content also decreases at all levels (supporting information Figure S2d).

In a convecting atmosphere, subcloud equivalent potential temperature θ_{eb} is an important quantity that covaries with upper-level temperature on time scales longer than that of variations in convective available potential energy (moist static energy or moist entropy are interchangeable with θ_{eb} for present purposes). This is the central tenet of convective quasi-equilibrium: convection acts on fast enough time scales that the large-scale dynamics interact only with a moist adiabatic temperature profile that covaries with θ_{eb}, greatly reducing the number of vertical degrees of freedom [*Emanuel et al.*, 1994]. In our model integrations, upper-level temperature indeed covaries with θ_{eb}. Moreover, variations in the saturation equivalent potential temperature of the convecting layer, θ_e^* (which is controlled only by temperature), are equal to variations in θ_{eb} (Figure 2c), which is sometimes called strict convective quasi-equilibrium [*Brown and Bretherton*, 1997; *Emanuel et al.*, 1994].

Given the tight covariation between θ_{eb} and upper tropospheric temperature, we use θ_{eb} to study the sensitivity of tropospheric temperature to surface elevation and albedo. Linear fits (Figure 2d) show that θ_{eb} changes at a rate of -8 K/100 hPa for the surface elevation control parameter and at a rate of -4.5 K/0.01 for the albedo control parameter (the denominator of the latter

202 expression is a dimensionless albedo change). When these linear sensitivities are multiplied,
203 respectively, by the observed differences in elevation (~400 hPa) and albedo (~0.07) between
204 India and Tibet, one obtains an estimate for the elevated heating effect over the plateau (+32 K)
205 that is roughly equal to the albedo-induced cooling (-31.5 K). This seems sufficient to explain
206 why the plateau is not observed to be site of the warmest upper-troposphere in South Asia.
207
208 Although the linear estimate for the sensitivity of θ_{eb} to surface albedo works well around the
209 albedo of 0.24 (that of the observed Tibetan Plateau), it underestimates the sensitivity at low
210 albedos (left-most crosses in Figure 2d). For CSRM simulations at even lower albedos, the
211 radiative-convective system achieves a runaway greenhouse regime [*Goldblatt and Watson*,
212 2012; *Ingersol*, 1969; *Kasting*, 1988] once albedo drops below a threshold. In those cases of high
213 longwave optical depth, the top-of-atmosphere incoming shortwave radiation exceeds the
214 maximum outgoing longwave radiation the moist column can have so that surface temperature
215 increases without bound [e.g. *Ingersol*, 1969; *Nakajima et al.*, 1992]. The albedo threshold for a
216 runaway greenhouse is about 0.16 for a surface at 4 km (Figure 3, which shows all the
217 experiments described herein together with some additional albedo-elevation combinations),
218 though it varies with surface elevation (e.g. it is about 0.2 for a non-elevated surface). The
219 observed summer surface albedo of much of India is lower than this threshold (Figure 1),
220 indicating that India would achieve a local runaway greenhouse state were it not for advection of
221 cooler and drier air into that region by the large-scale monsoonal flow [see also *Pierrehumbert*,
222 1995]. Thus, the nonlinear sensitivity of tropospheric temperature to surface albedo gives even
223 more dominance to the non-elevated part of India as a thermal maximum in RCE.
224
225 The strength of the elevated heating effect is not constant as climate changes. Our simulations
226 suggest that the RCE elevated heating effect is weaker in warmer climates. For example, when
227 the prescribed surface albedo decreases from 0.24 to 0.18 (which can be viewed as making the
228 background climate state warmer), elevated heating first gets weaker and then even changes its
229 sign to become elevated cooling, evidenced by the shift from a runaway greenhouse to a stable
230 RCE state as the surface is elevated (Figure 3). The detailed physics of orographic elevated
231 heating and why it becomes weaker in a warmer climate are discussed by *Hu and Boos* [2017].
232
233 **4. Discussion**
234
235 Here we explored competing effects of surface albedo and surface elevation on tropospheric
236 temperatures in radiative-convective equilibrium. We showed that, in non-polar regions, annual-
237 mean land surface albedo increases with surface elevation, especially above 3-4 km. This simple
238 observation suggests the possibility for orographic elevated heating to be compensated by
239 albedo-induced cooling. Simulations of the theoretical state of radiative-convective equilibrium
240 revealed a range of surface elevations and albedos over which the sensitivity of upper-
241 tropospheric temperature to each of these quantities was nearly linear; multiplying these linear
242 sensitivities by the observed differences in albedo and elevation between India and Tibet yielded
243 almost exact cancellation between orographic elevated heating and albedo-induced cooling for
244 those regions.
245
246 Nonlinearities at low albedos render elevated heating even less effective. In particular, surface
247 albedos of ~0.2 or less foster runaway greenhouse states, with this threshold albedo being higher

for lower surfaces. Although ventilation of these hot states by the large-scale circulation would prevent a runaway greenhouse, as might limited water availability over land, the tendency of low-elevation, low-albedo surfaces toward such hot states is exactly what drives the large-scale circulation. This lends more weight to the idea that non-elevated parts of India provide the dominant thermal forcing for the South Asian monsoon, with the primary effect of orography being to suppress intrusions of dry air into the thermal maximum [see review by *Boos*, 2015].

Hypotheses for South Asian monsoon changes over the past 50 million years have been based almost exclusively on changes in surface elevation [*An et al.*, 2001; *Molnar et al.*, 2010], but our results show that these must be considered jointly with changes in surface albedo (which covaries with land surface type). For example, lake and forest cover over Tibet may have been much greater during the warm Pliocene than they are now (a few examples are noted in Figure 1a) [*Chang et al.*, 2008; *Hsu*, 1983; *Igarashi et al.*, 1988; *Li et al.*, 2014; *Lu et al.*, 2001], resulting in a plateau with lower albedo but unchanged elevation. Upper-tropospheric temperature over the plateau may have thus been higher in the Pliocene due to the lower albedo, though this may have been countered by the reduction in elevated heating that occurs in warmer climates. Similar effects may occur in the future if mean temperatures rise and snow cover decreases over Tibet.

Even though our study is set in the context of the South Asian summer monsoon, it has potential implications for any low-latitude region with large topographic contrast, such as South America, North America, or even parts of Mars. The generality of our results is supported by the fact that Tibet and India lie near the median observed albedo in each elevation bin (Figure 1b). However, it is unclear whether there is any universal constraint on the albedo-elevation relationship. For example, does the fact that water rains out as air ascends along orographic slopes reduce surface water availability over plateaus and thus increase their albedo? How much of the albedo-elevation relationship is set by snow or ice cover? Given the difficulty of reconstructing the surface albedo of past climate states, these questions may be crucial for understanding the evolution of continental climate on geological timescales.

This study focused on idealized states in which radiative-convective processes alone determine the time-mean temperature. Caveats thus abound, including those associated with our use of idealized insolation without an annual or diurnal cycle. Nevertheless, our RCE paradigm provides a sense of what the climate might look like in the absence of a large-scale circulation. Feedbacks between the large-scale circulation and radiative-convective processes are expected to occur [e.g. *Nilsson and Emanuel*, 1999], but the large-scale circulation might be at least roughly thought of as a response to the RCE basic state. For example, *Pierrehumbert* [1995] discussed how radiation of energy to space through dry, subsiding parts of the atmosphere prevents moist tropical regions from achieving what would otherwise be a runaway greenhouse state. The role of clouds in interactions with the large-scale circulation also deserves further investigation, even though observed longwave and shortwave cloud radiative effects seem to largely cancel out in tropical regions (e.g. supporting information Figure S4). The field of climate dynamics has made progress in thinking about such interactions between radiation, moist convection, and large-scale flow, but these interactions need to be better understood in continental regions with large contrasts in surface albedo and elevation.

Acknowledgements

We acknowledge support from National Science Foundation grants AGS-1253222 and AGS-1515960, Office of Naval Research grant N00014-15-1-2531, and the Yale University Faculty of Arts and Sciences High Performance Computing facility. We thank Peter Molnar and Mark Brandon for helpful discussions. The data used in this study are available upon request from the authors (shineng.hu@yale.edu).

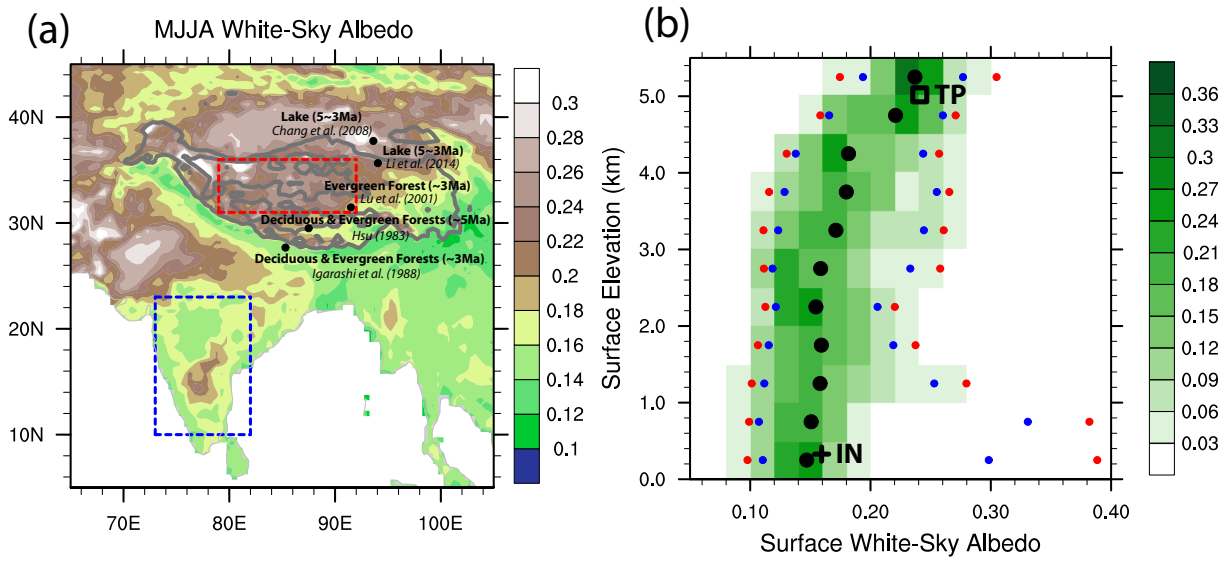

Figure 1: (a) May-August climatological mean white-sky land surface albedo. Black dots mark sites where land surface types were reconstructed for the warm Pliocene in previous work. Gray contours mark elevations of 4 km and 5 km above sea level. (b) Annual mean albedo-elevation diagram for all land 60°S-60°N. Each land point was binned by its surface elevation (with a bin size of 0.5 km), and a histogram of surface albedo was compiled for each elevation bin (with an albedo bin size of 0.02). Green shading shows the fraction of points in each elevation bin that falls in a given albedo bin, black dots mark the median albedo in each elevation bin, and blue and red dots respectively mark the 10-90% and 5-95% range of albedo in each elevation bin. The black square and cross mark observed annual mean values for the Tibetan Plateau (TP) and the Indian region (IN), respectively, which are outlined by the red and blue rectangles in (a).

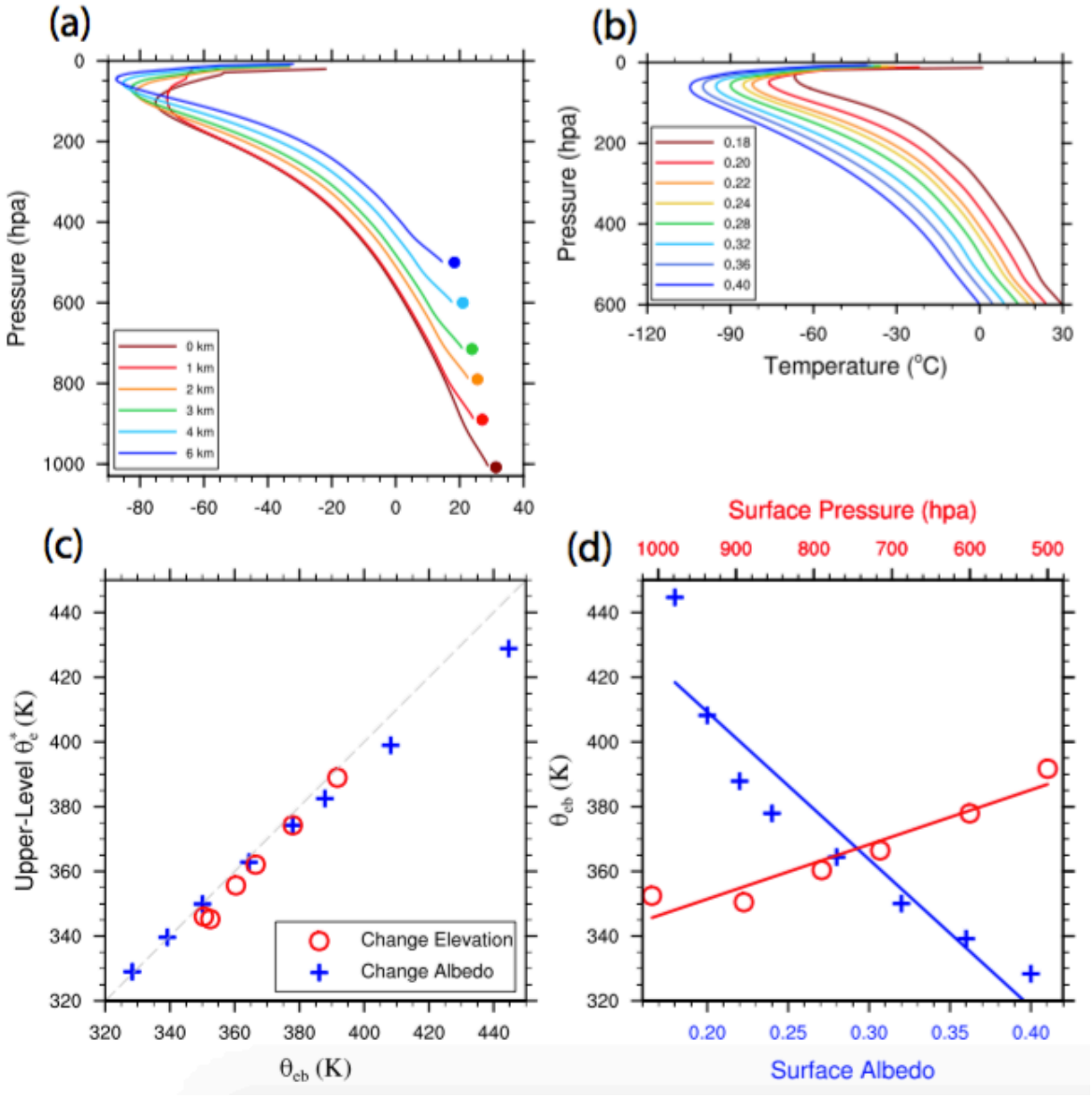

Figure 2: (a, b) Equilibrium temperature profiles from cloud system-resolving simulations with (a) various surface elevations but the same surface albedo of 0.24, and with (b) various surface albedos but the same surface elevation of ~4 km. In panel (a), colored dots indicate the surface temperature for the corresponding case. (c) Upper tropospheric (200-400 hPa) saturation equivalent potential temperatures versus subcloud (25 hPa above surface) equivalent potential temperatures for the simulations shown in panels (a,b). The gray dashed one-to-one line corresponds to the strict convective quasi-equilibrium assumption. (d) Sensitivities of subcloud equivalent potential temperatures to surface albedos and surface elevations for the simulations shown in panels (a,b), with best linear fits. Panels (a,c) are reproduced and modified from *Hu and Boos* [2016].

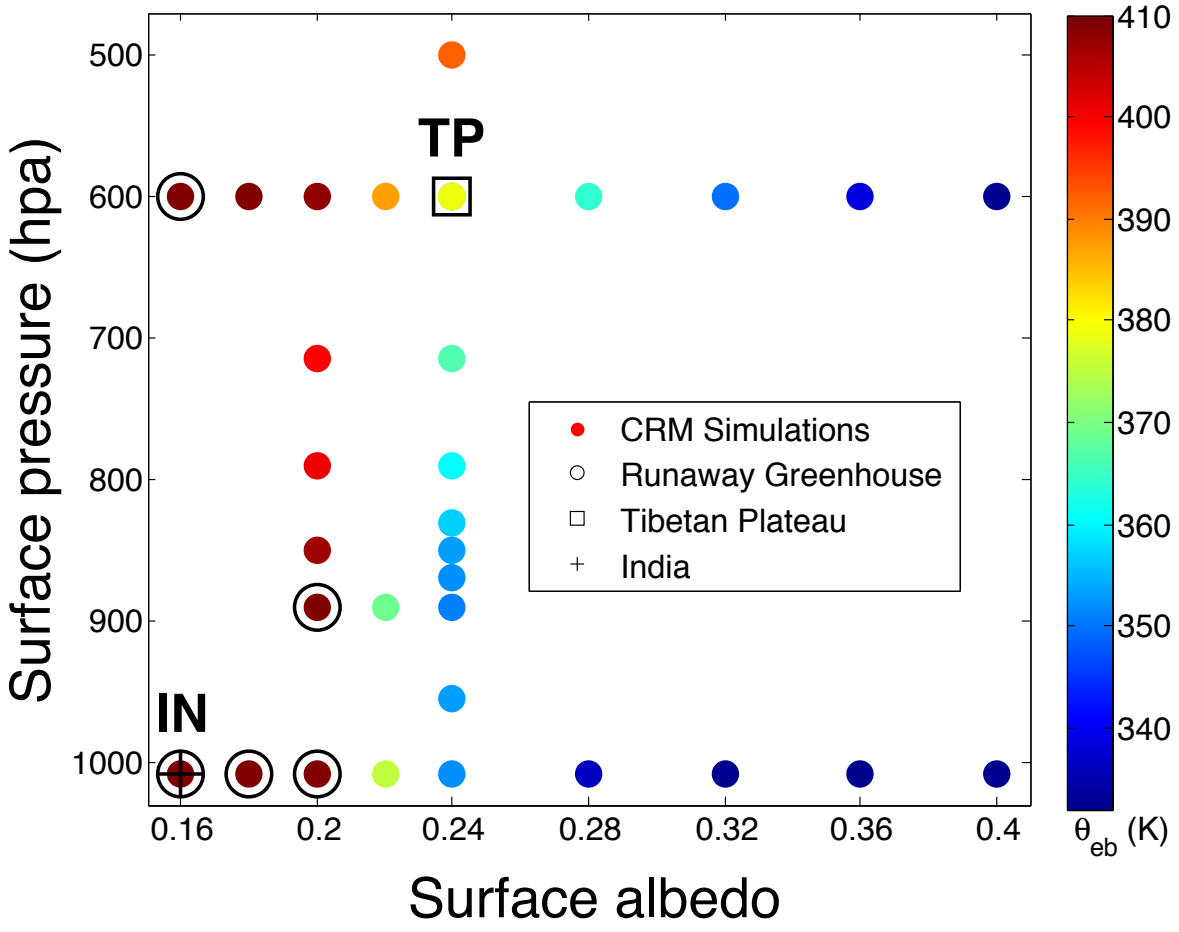

Figure 3: The color of each dot indicates the subcloud (25 hPa above the surface) equivalent potential temperature of the radiative-convective equilibrium state simulated by our cloud system-resolving model at the given combination of surface pressure and surface albedo. Black circles surround dots for simulations that enter a runaway greenhouse regime. The black square and cross mark the cases with surface albedos and elevations most similar to those of the Tibetan Plateau (TP) and Indian region (IN), respectively.

References

Amante, C., and B. W. Eakins (2009), *ETOPO1 1 arc-minute global relief model: procedures, data sources and analysis*, US Department of Commerce, National Oceanic and Atmospheric Administration, National Environmental Satellite, Data, and Information Service, National Geophysical Data Center, Marine Geology and Geophysics Division.

An, Z. S., J. E. Kutzbach, W. L. Prell, and S. C. Porter (2001), Evolution of Asian monsoons and phased uplift of the Himalayan Tibetan plateau since Late Miocene times, *Nature*, *411*(6833), 62-66.

Boos, W. R. (2015), A review of recent progress on Tibet's role in the South Asian monsoon. *CLIVAR Exchanges Special Issue on Monsoons*, 66, 23-27.

Boos, W. R., and Z. M. Kuang (2010), Dominant control of the South Asian monsoon by orographic insulation versus plateau heating, *Nature*, *463*(7278), 218-222.

Brown, R. G., and C. S. Bretherton (1997), A test of the strict quasi-equilibrium theory on long time and space scales, *J. Atmos. Sci.*, *54*(5), 624-638.

Caballero, R. (2012), CliMT: Climate Modeling and Diagnostics Toolkit. [Available online at https://github.com/rodrigo-caballero/CliMT.]

Chakraborty, A., R. S. Nanjundiah, and J. Srinivasan (2002), Role of Asian and African orography in Indian summer monsoon, *Geophys. Res. Lett.*, 29(20), 1989.

Chakraborty, A., R. S. Nanjundiah, and J. Srinivasan (2006), Theoretical aspects of the onset of Indian summer monsoon from perturbed orography simulations in a GCM, *Ann. Geophys.*, 24, 2075-2089.

Chang, M. M., X. M. Wang, H. Z. Liu, D. S. Miao, Q. H. Zhao, G. X. Wu, J. Liu, Q. Li, Z. C. Sun, and N. Wang (2008), Extraordinarily thick-boned fish linked to the aridification of the Qaidam Basin (northern Tibetan Plateau), *P. Natl. Acad. Sci. U.S.A.*, *105*(36), 13246-13251.

Charney, J. G. (1975), Dynamics of deserts and drought in the Sahel, *Q. J. Roy. Meteor. Soc.*, *101*(428), 193-202.

Emanuel, K. A. (1994), *Atmospheric convection*, Oxford University Press.

Emanuel, K. A., J. D. Neelin, and C. S. Bretherton (1994), On Large-Scale Circulations in Convecting Atmospheres, *Q. J. Roy. Meteor. Soc.*, *120*(519), 1111-1143.

Flohn, H. (1953), Hochgebirge und allgemeine Zirkulation. II. Die Gebirge als Wa¨rmequellen. *Arch. Meteorol. Geophys. Bioklimatol.*, A 5, 265–279.

Flohn, H. (1968), *Contributions to a meteorology of the Tibetan Highlands*, Department of Atmospheric Science, Colorado State University.

Friedl, M. A., et al. (2002), Global land cover mapping from MODIS: algorithms and early results, *Remote Sens. Environ.*, *83*(1), 287-302.

Goldblatt, C., and A. J. Watson (2012), The runaway greenhouse: implications for future climate change, geoengineering and planetary atmospheres, *Philos. T. R. Soc. A*, *370*(1974), 4197-4216.

Hahn, D. G., and S. Manabe (1975), Role of Mountains in South Asian Monsoon Circulation, *J. Atmos. Sci.*, *32*(8), 1515-1541.

Hsu, J. (1983), Late Cretaceous and Cenozoic Vegetation in China, Emphasizing Their Connections with North-America, *Ann. Mo. Bot. Gard.*, *70*(3), 490-508.

Hu, S., and W. R. Boos (2017), On the physics of orographic elevated heating in radiative-convective equilibrium, in review at *J. Atmos. Sci.*, http://people.earth.yale.edu/sites/default/files/files/Boos/HB16_JAS_submitted.pdf

Igarashi, Y., M. Yoshida, and H. Tabata (1988), History of vegetation and climate in the Kathmandu Valley, *P. of Indian Natl. Sci. Acad.*, 4, 212-225.

Ingersol, A. P. (1969), Runaway Greenhouse - a History of Water on Venus, *J. Atmos. Sci.*, *26*(6), 1191-1198.

Jin, Y., C. B. Schaaf, C. E. Woodcock, F. Gao, X. Li, A. H. Strahler, W. Lucht, and S. Liang (2003), Consistency of MODIS surface bidirectional reflectance distribution function and albedo retrievals: 2. Validation. *J. Geophys. Res.-Atmos.*, *108*(D5).

Kasting, J. F. (1988), Runaway and Moist Greenhouse Atmospheres and the Evolution of Earth and Venus, *Icarus*, *74*(3), 472-494.

Khairoutdinov, M. F., and D. A. Randall (2003), Cloud resolving modeling of the ARM summer 1997 IOP: Model formulation, results, uncertainties, and sensitivities, *J. Atmos. Sci.*, *60*(4), 607-625.

Kiehl, J. T., J. J. Hack, G. B. Bonan, B. A. Boville, D. L. Williamson, and P. J. Rasch (1998), The National Center for Atmospheric Research Community Climate Model: CCM3. *J. Climate*, 11, 1131-1149

Li, Q., G. P. Xie, G. T. Takeuchi, T. Deng, Z. J. Tseng, C. Grohe, and X. M. Wang (2014), Vertebrate fossils on the roof of the world: Biostratigraphy and geochronology of high-elevation Kunlun Pass Basin, northern Tibetan Plateau, and basin history as related to the Kunlun strike-slip fault, *Palaeogeogr. Palaeocl.*, *411*, 46-55.

Lindzen, R. S., and A. Y. Hou (1988), Hadley Circulations for Zonally Averaged Heating Centered Off the Equator, *J. Atmos. Sci.*, *45*(17), 2416-2427.

Lu, H. Y., S. M. Wang, N. Q. Wu, G. B. Tong, X. D. Yang, C. M. Shen, S. J. Li, L. P. Zhu, and L. Wang (2001), A new pollen record of the last 2.8 Ma from the Co Ngoin, central Tibetan Plateau, *Sci. China Ser. D*, *44*, 292-300.

Ma, D., W. Boos, and Z. Kuang (2014), Effects of Orography and Surface Heat Fluxes on the South Asian Summer Monsoon, *J. Climate*, 27(17), 6647-6659.

Molnar, P., and K. A. Emanuel (1999), Temperature profiles in radiative-convective equilibrium above surfaces at different heights, *J. Geophys. Res.-Atmos.*, *104*(D20), 24265-24271.

Molnar, P., P. England, and J. Martinod (1993), Mantle Dynamics, Uplift of the Tibetan Plateau, and the Indian Monsoon, *Rev. Geophys.*, *31*(4), 357-396.

Molnar, P., W. R. Boos, and D. S. Battisti (2010), Orographic Controls on Climate and Paleoclimate of Asia: Thermal and Mechanical Roles for the Tibetan Plateau, *Annu. Rev. Earth Pl. Sc.*, *38*, 77-102.

Moody, E. G., M. D. King, S. Platnick, C. B. Schaaf, and F. Gao (2005), Spatially complete global spectral surface albedos: Value-added datasets derived from terra MODIS land products, *Ieee T. Geosci. Remote*, *43*(1), 144-158.

Nakajima, S., Y.-Y. Hayashi, and Y. Abe (1992), A study of the 'runaway greenhouse effect' with a one-dimensional radiative-convective model. *J. Atmos. Sci.* 49, 2256–2266.

Nie, J., W. R. Boos, and Z. M. Kuang (2010), Observational Evaluation of a Convective Quasi-Equilibrium View of Monsoons, *J. Climate*, *23*(16), 4416-4428.

Nilsson, J., and K. A. Emanuel (1999), Equilibrium atmospheres of a two-column radiative-convective model. *Q. J. Roy. Meteor. Soc.*, 125(558), 2239-2264.

425 Pierrehumbert, R. T. (1995), Thermostats, radiator fins, and the local runaway greenhouse. *J.*
426 *Atmos. Sci.*, 52(10), 1784-1806.
427 Rao, G. V., and S. Erdogan (1989), The Atmospheric Heat-Source over the Bolivian Plateau for
428 a Mean January, *Bound.-Lay. Meteorol.*, *46*(1-2), 13-33.
429 Richardson, M. I., and R. J. Wilson (2002), A topographically forced asymmetry in the martian
430 circulation and climate, *Nature*, *416*(6878), 298-301.
431 Schneider, T. (2006), The general circulation of the atmosphere, *Annu. Rev. Earth Pl. Sc.*, *34*,
432 655-688.
433 Staff Members of Academia Sinica (1958), On the General Circulation over Eastern Asia III,
434 *Tellus*, *10*(3), 299-312.
435 Tang, M. C., and E. R. Reiter (1984), Plateau Monsoons of the Northern Hemisphere - a
436 Comparison between North-America and Tibet, *Mon. Weather Rev.*, *112*(4), 617-637.
437 Wang, K., J. Liu, X. Zhou, M. Sparrow, M. Ma, Z. Sun, and W. Jiang (2004), Validation of the
438 MODIS global land surface albedo product using ground measurements in a semidesert
439 region on the Tibetan Plateau. *J. Geophys. Res.-Atmos.*, *109*(D5).
440 Wu, G. X., Y. M. Liu, B. He, Q. Bao, A. M. Duan, and F. F. Jin (2012), Thermal Controls on the
441 Asian Summer Monsoon, *Sci. Rep.*, 2, 404.
442 Wu, G. X., Y. M. Liu, T. M. Wang, R. J. Wan, X. Liu, W. P. Li, Z. Z. Wang, Q. Zhang, A. M.
443 Duan, and X. Y. Liang (2007), The influence of mechanical and thermal forcing by the
444 Tibetan Plateau on Asian climate, *J. Hydrometeorol.*, *8*(4), 770-789.
445 Yanai, M., and G. X. Wu (2006), Effects of the Tibetan Plateau, in *The Asian Monsoon*, edited
446 by B. Wang, Springer, 513–549.
447 Zaitchik, B. F., J. P. Evans, and R. B. Smith (2007), Regional impact of an elevated heat source:
448 The Zagros Plateau of Iran, *J. Climate*, *20*(16), 4133-4146.

Supporting Information for

Competing effects of surface albedo and orographic elevated heating on regional climate

Shineng Hu and William R. Boos

Department of Geology and Geophysics, Yale University, New Haven, CT 06511, USA

Contents of this file

Figures S1-**S4**

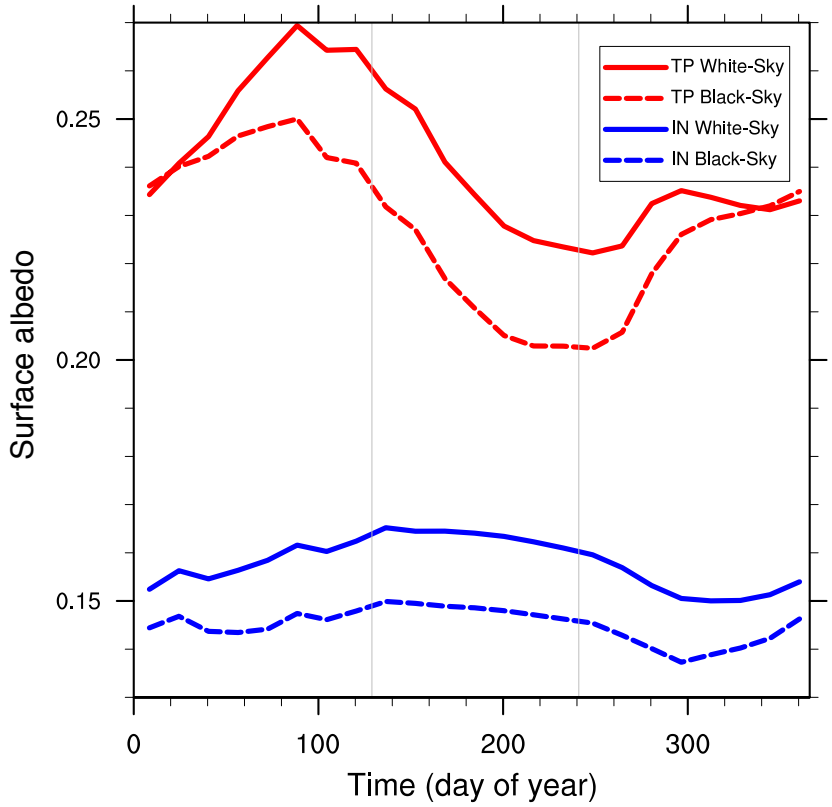

Figure S1: Seasonal variations in white-sky (solid lines) and black-sky (dashed lines) surface albedo for the Tibetan Plateau (TP; red lines) and the Indian region (IN; blue lines). The TP and the IN albedos are obtained by averaging over the red and blue dashed boxes, respectively, in Figure 1a. Vertical gray lines mark the core South Asian summer monsoon season (roughly May-August) that is used to calculate temporal average for Figure 1a.

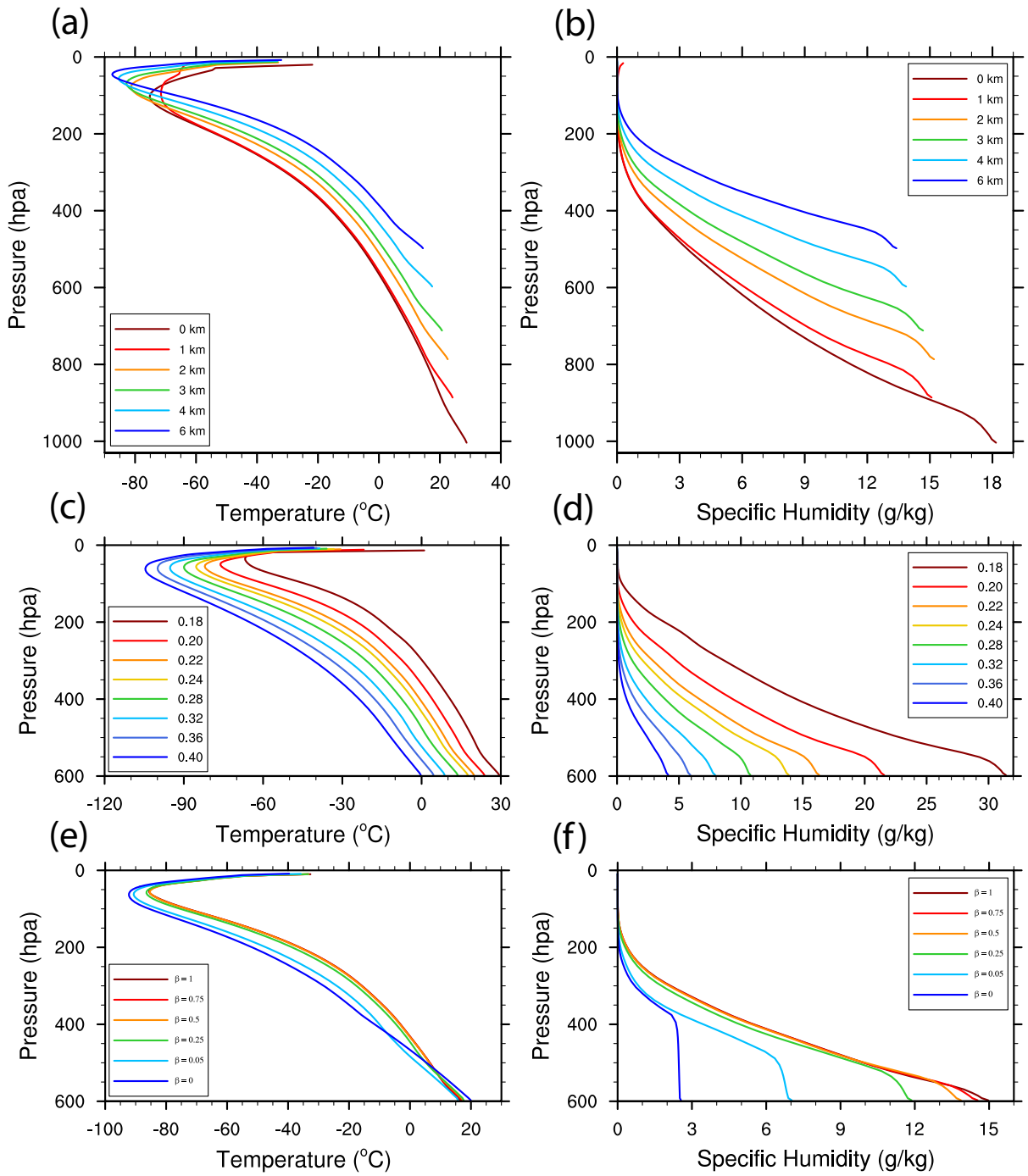

Figure S2: Radiative-convective equilibrium profiles from the cloud system-resolving simulations. Profiles of temperature (°C; left) and specific humidity (g/kg; right) for the sets of simulations with varied (a,b) surface pressures, (c,d) surface albedos, and (e,f) surface evaporative fractions. In each set, other than the parameter that is varied, other parameters are fixed at a value of 600 hPa for surface pressure, 0.24 for surface albedo, and 0.5 for evaporative fraction.

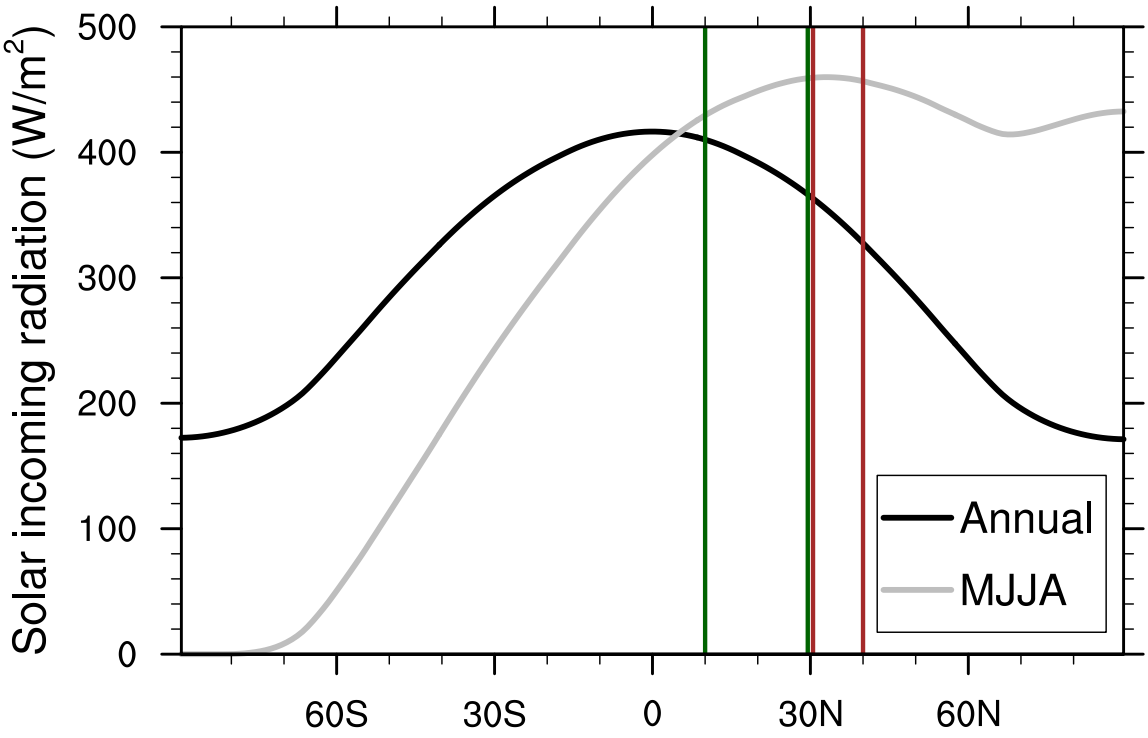

Figure S3: Limited zonal means of insolation (W/m^2) as a function of latitude over the regional boxes shown in Fig. 1. The black line is for annual mean conditions, while the grey line is for boreal summer mean (May through August). The paired brown and green vertical lines mark the approximate latitudinal boundaries for the Tibetan Plateau (10°N-30°N) and the Indian subcontinent (30°N-40°N), respectively. Data used are from the Clouds and the Earth's Radiant Energy System (CERES) product.

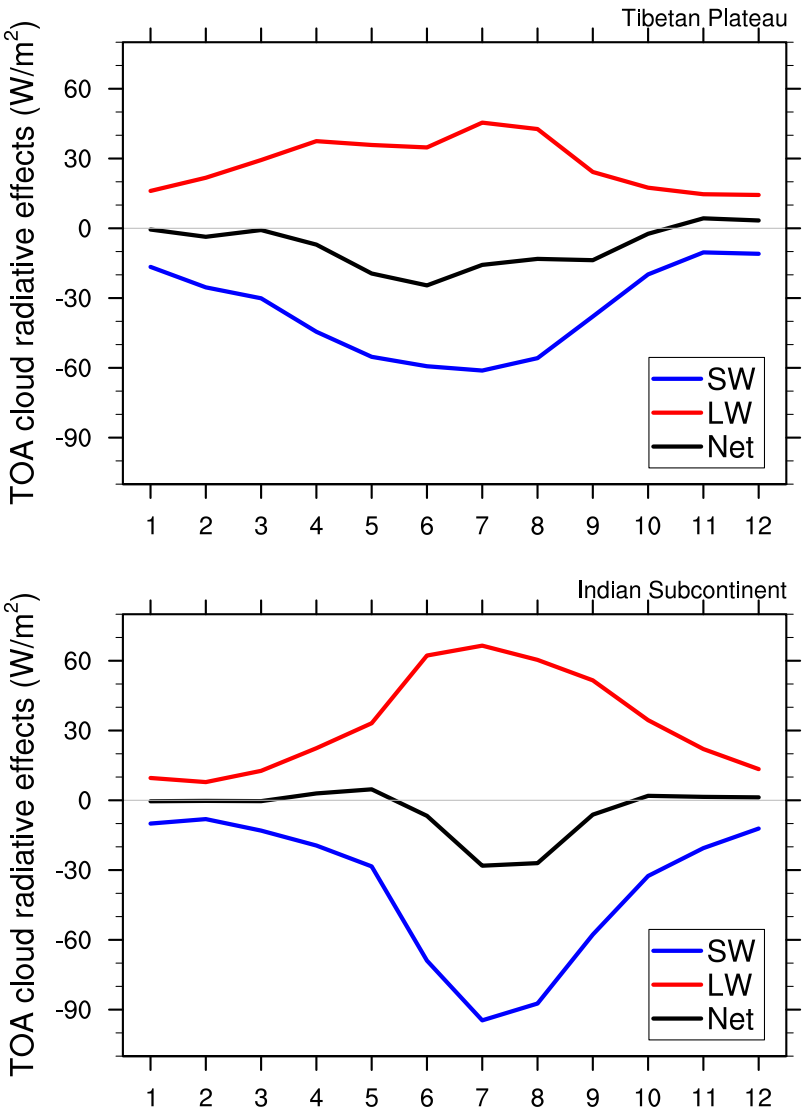

Figure S4: Climatological mean seasonal cycle of top-of-atmosphere (TOA) cloud radiative effects (W/m^2) over (top) the Tibetan Plateau and (bottom) the Indian subcontinent, as averaged within the red and blue boxes in Fig. 1, respectively. Numbers (1,2,…,12) on the horizontal axis represent months (January, February, …, December), 'SW' and 'LW' represent shortwave and longwave, respectively, and 'Net' represents the sum of both. Data are from the CERES product.